View metadata, citation and similar papers at core.ac.uk

brought to you by CORE

provided by IntechOpen

We are IntechOpen, the world's leading publisher of Open Access books Built by scientists, for scientists

4,800
Open access books available

122,000
International authors and editors

135M
Downloads

Our authors are among the

154
Countries delivered to

TOP 1%
most cited scientists

12.2%
Contributors from top 500 universities

CLARIVATE ANALYTICS BOOK CITATION INDEX INDEXED

WEB OF SCIENCE™

Selection of our books indexed in the Book Citation Index in Web of Science™ Core Collection (BKCI)

Interested in publishing with us?
Contact book.department@intechopen.com

Numbers displayed above are based on latest data collected.
For more information visit www.intechopen.com

4

Dynamics of Magnetic Relaxation in Spheromaks

Pablo L. Garcia-Martinez
[1]*Laboratoire de Physique des Plasmas, Ecole Polytechnique, Palaiseau cedex*
[2]*CONICET and Centro Atómico Bariloche (CNEA), San Carlos de Bariloche*
[1]*France*
[2]*Argentina*

1. Introduction

The first attempts to get energy from the controlled fusion of two light atoms nuclei date back to the beginning of the fifties of the last century. The crucial difficulty to achieve this goal is that particles need to have a large amount of thermal energy in order to have a significant chance of overcoming the Coulomb repulsion. At such high temperatures the atoms are fully ionized conforming a plasma. Such a hot plasma can not be in contact with solid walls because it will be rapidly cooled down. Two main methods have been developed to confine plasmas: the magnetic confinement and the inertial confinement. Here we are concerned with the magnetic confinement approach.

Under certain conditions some magnetic configurations studied in the context of plasma confinement become unstable and undergo a process called magnetic (or plasma) relaxation. This process generally causes the system to evolve toward a self-organized state with lower magnetic energy and almost the same magnetic helicity. A key physical mechanism that operates during plasma relaxation is the localized reconnection of magnetic field lines. It was demonstrated that magnetic relaxation can be employed to form and sustain configurations relevant to magnetic confinement research.

The theoretical description of magnetic relaxation is given in terms of a variational principle (Taylor, 1974). Despite the remarkable success of this theory to describe the final self-organized state toward which the plasma evolves, it does not provide any information on the dynamics of the plasma during relaxation. Since the process of relaxation always involves fluctuations that degrade plasma confinement it is very important to understand their dynamics.

The dynamics of the fluctuations induced during the relaxation process can be studied in the context the magnetohydrodynamic (MHD) model. In this Chapter, we will study the dynamics of the relaxation in kink unstable spheromak configurations. To that end we will solve the time-dependent non-linear MHD equations in three spatial dimensions.

The rest of the Chapter is organized as follows. In Section 2 we give a general introduction to magnetic confinement of high temperature plasma which is the main motivation of this study. The physical background of this work is the MHD model which is presented in Section 3. In Section 4 we describe the magnetic relaxation theory and its relationship with

plasma self-organization. The role of the magnetic helicity and magnetic reconnection is also discussed. In Section 5 we present a study of the dynamics of magnetic relaxation in kink unstable spheromak configurations. These configurations are of special interest because they approximate quite well the measurements in spheromaks during sustainment (Knox et al., 1986);(Willet et al., 1999). Previous works have shown the existence of a partial relaxation behavior in marginally unstable configurations (Garcia-Martinez & Farengo, 2009a); (Garcia-Martinez & Farengo, 2009b). In this work we analyze this process in detail and we show, in particular, that this behaviour is connected to the presence of a rational surface near the magnetic axis. The main conclusions are summarized in Section 6.

2. Magnetic confinement of high temperature plasmas

The charged particles which constitute a high temperature plasma are subjected to the Lorentz force. The objective of magnetic confinement is to create magnetic field configurations to constrain the motion of the particles trying to keep them trapped far from the container's wall. In order to accomplish this goal the following four conditions must be fulfilled:

1. The configuration must be in magnetohydrodynamic (MHD) equilibrium.
2. The configuration must be stable (or it should be possible to mitigate or control potential instabilities).
3. Methods to produce, heat and sustain the configuration must be available.
4. The losses due to transport of heat and particles must be low enough to allow the system to have an adequate confinement time.

Here we will discuss some general aspects of the first three points. A more detailed discussion on these topics may be found, for instance, in the book of Wesson (2004).

2.1 MHD equilibrium

It is said that a magnetic configuration is in static MHD equilibrium if the Lorentz force cancels out exactly the pressure force

$$\mathbf{J} \times \mathbf{B} = \nabla p. \tag{1}$$

This force balance is part of the momentum equation of the MHD model that will be presented in Sec. 3. The magnetic configurations employed for plasma confinement almost always have toroidal topology. In this situation, each magnetic field line describes a toroidal magnetic surface. These toroidal magnetic surfaces are nested around a circle called magnetic axis (see Fig. 1). The separatrix is the outermost closed surface that does not touch the vessel. Three axisymmetric toroidal configuration schemes are shown in Fig. 1. It is a common practice to decompose the magnetic field into its toroidal and poloidal components. If we place a cylindrical coordinate system at the center of the torus, aligning the z-axis with the axis of symmetry (of revolution) of the torus, the toroidal direction coincides with the azimuthal direction and the poloidal plane lies in the r-z plane. In the right column of Fig. 1 we show the profiles of the toroidal and poloidal magnetic fields as a function of the distance between the magnetic axis and the separatrix for each configuration. Let's review the main features of these configurations.

- Tokamak. The toroidal magnetic field is much larger than the poloidal one. This intense toroidal field is imposed by a set of large external coils while the poloidal field comes from

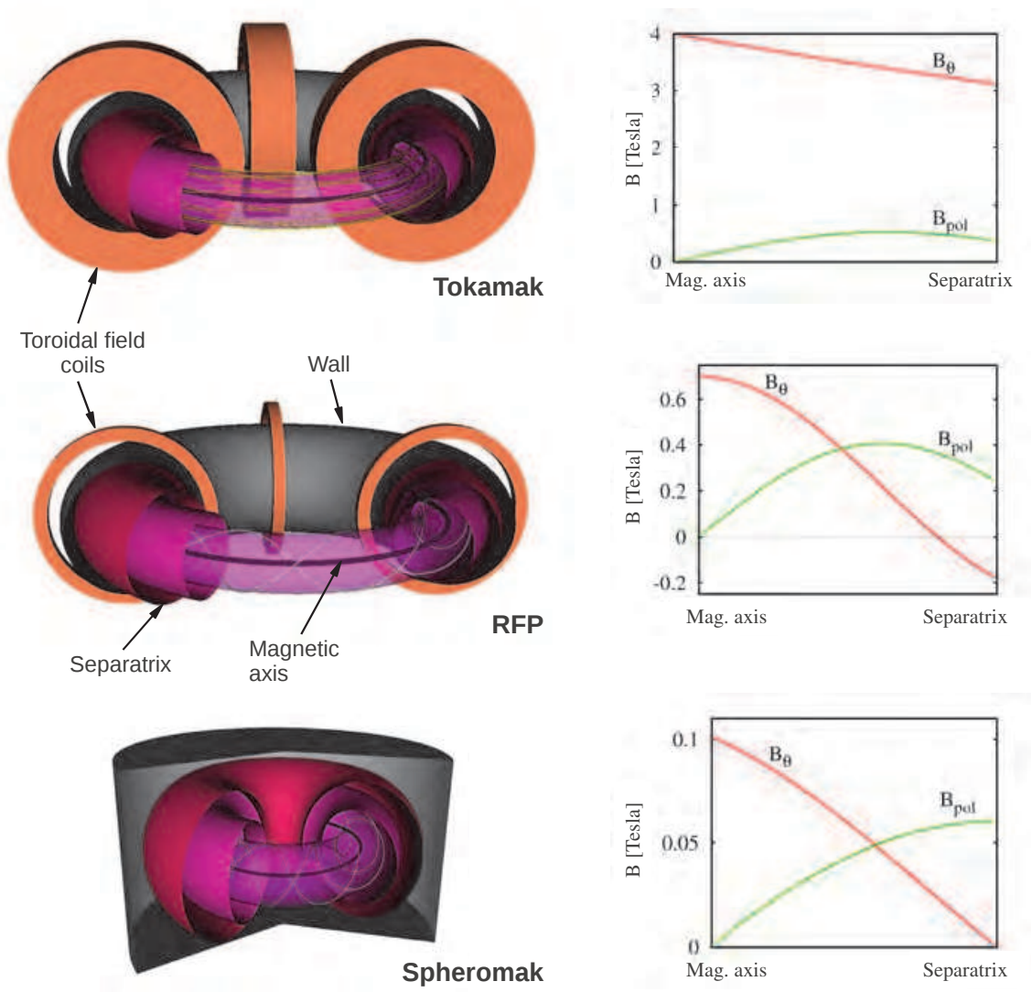

Fig. 1. Three examples of toroidal axisymmetric configurations used in magnetic confinement research: the tokamak, the reversed field pinch (RFP) and the spheromak.

the toroidal current that flows through the plasma. Typically, this current is produced by the electric field induced by the temporal variation of the magnetic flux linked by the torus.

- RFP (reversed field pinch). It is also an axisymmetric toroidal device whose aspect ratio (ratio of the major radius and the minor radius of the torus) is generally larger than that of the tokamak. The toroidal and poloidal fields have similar strengths. This makes the system much more prone to develop MHD instabilities. The magnetic field generation is analogous to that of the tokamak but using smaller coils for the toroidal field. The toroidal field reverses (changes its sign) near the separatrix opposing the externally applied field as a result of a magnetic relaxation process.
- Spheromak. It belongs to the family of compact tori. These are toroidal magnetic configurations formed inside a simply connected volume. The lack of elements being linked by the plasma represents a great advantage from a constructive and economical point of view. The two components of the magnetic field have similar strength. This

configuration is formed as a result of a relaxation process that self-organizes the magnetic field, closely related to that occurring in the RFP.

In all these three systems as well as in other important configurations the magnetic surfaces spanned by the magnetic field lines play a central role in confinement. We examine this in more detail. Let $\psi(r,z)$ be the poloidal flux function defined as

$$\psi(r,z) = \int_{S(r,z)} \mathbf{B} \cdot d\mathbf{s} \tag{2}$$

were $S(r,z)$ is the circle of radius r centered at the position z of the vertical axis. If the configuration is axisymmetric we can express the poloidal flux function as

$$\psi(r,z) = 2\pi \int_0^r B_z(\chi,z)\, \chi d\chi. \tag{3}$$

With this definition ψ reaches its maximum value at the magnetic axis ($\psi(r_{\mathrm{ma}}, z_{\mathrm{ma}}) = \psi_{\mathrm{ma}}$). The magnetic surfaces, or flux surfaces, can be determined by the equation $\psi(r,z) = C$ where C is a constant. Note that this useful labeling system for the flux surfaces breaks down when the axisymmetry is lost (due to an instability for example).

The poloidal flux function acts as a stream function for the poloidal field since

$$\mathbf{B}_p = \nabla \times \left(\frac{\psi(r,z)}{2\pi r} \hat{\theta} \right) \tag{4}$$

where $\hat{\theta}$ is the unit vector pointing in the toroidal direction. Note that the poloidal flux function is closely related to the toroidal component of the magnetic vector potential $\mathbf{A}$ since Eq. (4) implies that

$$\psi = 2\pi r A_\theta. \tag{5}$$

This relationship has important consequences for the confinement of the plasma particles. Due to the axisymmetry, the canonical angular momentum $P_\theta = mrv_\theta + qrA_\theta$ turns out to be a constant of the motion of each particle (m and Ze being the mass and the charge of the particle, respectively). In terms of the poloidal flux we can see that

$$P_\theta = mrv_\theta + \frac{Ze}{2\pi}\psi \tag{6}$$

is a constant of motion. If the magnetic field is strong enough the term mrv_θ may become very small compared with $Ze\psi/(2\pi)$. In that case the particles are constrained to move along surfaces of constant ψ, i.e. along magnetic surfaces. For this reason, an effective way of confining charged particles can be obtained by creating a set of nested toroidal magnetic surfaces. The rupture of flux surfaces caused by asymmetries in the field generation or instabilities certainly has a detrimental effect on confinement.

2.2 Stability

An equilibrium is unstable if it is possible to find a small perturbation that growths when is applied. Otherwise, the equilibrium is stable. The instabilities observed in

magnetically confined plasmas can be classified into two groups: the microinstabilities and the macroinstabilities. The first group is responsible for the turbulence at small scales and it is generally related to finite Larmor radius effects (the gyroradius of charged particles turning around the magnetic field) and asymmetries in the velocity distribution function of the different species that compound the plasma. On the other hand, the macroinstabilities involve fluctuations having a length scale comparable to that of the whole system and can, in their simplest version, be described by the MHD model presented in Section 3. Their appearance generally leads to the termination of the discharge and the destruction of the configuration. In this Chapter we will deal with this kind of instabilities.

The usual procedure to study the MHD stability of an equilibrium is based on the analysis of the energy increment δW introduced by a small perturbation to the equilibrium (Friedberg, 1987). Using the linearized equations of the MHD model it is possible to compute the growth rate of each perturbation. If all possibles modes decay then the equilibrium is MHD stable.

According to the source of energy that feeds the instability, the macroinstabilities can be divided in:

- External modes. In this case the energy of the instability comes from the interaction between the plasma and the boundary (the separatrix) or the external magnetic fields. Two typical examples appearing in spheromaks are the shift and the tilt instabilities. The first one consists in the displacement of the configuration as a whole while the second one involves the rigid rotation of the magnetic surfaces. The flux conserver (the chamber of conducting walls inside which the spheromak is formed) plays a crucial role in suppressing these instabilities. For instance, in a cylindrical flux conserver the tilt instability can be avoided if the elongation of the cylinder (ratio between height and radius) is lower than 1.6.
- Current driven modes. They are activated by non uniform current distributions. The most common example of this kind of instabilities is the kink mode, which may be either an internal (it does not affect the separatrix) or an external mode. In tokamaks this instability is closely related to a phenomenon called sawtooth oscillations that limits in practice the maximum value of toroidal current. In spheromaks and RFP's the kink mode triggers the relaxation process that forms and sustains the configuration.
- Pressure modes. Pressure gradients combined with an adverse magnetic field line curvature may act as a source of energy to develop instabilites (called ballooning or interchange modes).

In Section 5 we will consider internal kink modes in spheromak configurations. A comprehensive description of the MHD modes relevant to magnetic confinement configurations can be found elsewhere (Friedberg, 1987);(Wesson, 2004).

2.3 Formation and sustainment

Once an MHD equilibrium with good stability properties has been devised it is necessary to find appropriate methods to form and sustain the configuration. The formation methods depend on the configuration under consideration. In fact, a given configuration can be obtained using different formation schemes. In most cases, after the formation process the plasma has a temperature sensibly lower than that required for fusion. Moreover, the resistive

dissipation which is ubiquitous on real plasmas causes the currents and the magnetic fields to decay, so the configuration would be lost in the resistive time scale. It is then imperative to apply adequate methods to drive currents and heat the plasma. Some common methods that have already been successfully implemented are:

- Current induction by a primary coil. A primary coil is located at the center of the torus and plays the role of the primary of an electric transformer while the plasma itself is the secondary (the primary coil was not sketched in Fig. 1). This is the usual approach to induce the toroidal current in tokamaks and RFP's. It does not allow to operate in truly steady state and it can not be used in compact tori.
- Radio frequency waves. Energy can be transferred to the plasma from an external source of electromagnetic waves (antenna). The electric field of the waves transfers momentum to the particles inducing currents and heating the plasma by collisions. Within a multi-species plasma there exists a number of resonant frequencies that enhance the coupling between the plasma and the antenna (ionic and electronic cyclotron resonances, hybrid resonances, etc.).
- Neutral beam injection. Neutral atoms injected are not deflected by the magnetic field and can penetrate the plasma until they become ionized through collisions. Once ionized these particles follow orbits determined by the magnetic field and their energy. This process heats the plasma and drives localized currents.
- Rotating magnetic fields. Plasma electrons may be dragged, and thus a current may be induced, by externally applied rotating magnetic fields.
- Helicity injection. When a current is established along the magnetic field some amount of magnetic helicity (see Sec. 4) is injected in the magnetic configuration. The driven current may destabilize the configuration triggering a relaxation process that redistributes the current. This is the main method used in spheromak sustainment and is the subject of study of this Chapter.

2.4 The spheromak configuration

Early experiments in toroidal pinch configurations exhibited, under certain conditions, the spontaneous reversal of the toroidal field near the wall of the chamber. This unexpected feature was succesfully explained in terms of the relaxation theory proposed by Taylor (1974). According to this theory, MHD fluctuations cause the plasma to minimize its magnetic energy while conserving the total magnetic helicity (see Sec. 4).

Some years later, it was realized that the minimum energy state, for a given amount of magnetic helicity, inside a sphere is a system of nested toroidal magnetic flux surfaces (Rosenbluth & Bussac, 1979). The idea of a configuration relevant for fusion research that would be self produced (or self-organized) inside a simply connected volume attracted the attention of the scientific community. Several experiments were designed in order to check this theoretical prediction. The success of these experiments was considered a proof of the remarkable robustness of the relaxation theory (Bellan, 2000).

Despite the initial enthusiasm, it was later realized that the relaxation process involves MHD fluctuations that strongly degrade the confinement. Because of these fluctuations the confinement peformance of the spheromak is much lower than that of the tokamak or the

RFP. Little is known about the dynamics of these fluctuations since the relaxation theory is only able to predict the final state of the plasma but it can not provide any detail on how this state is attained (Jarboe, 2005).

3. The MHD model

The MHD model describes the macroscopic behavior of a plasma in many situations of interest in a relatively simple manner. Its validity relies, however, in a number of assumptions that have to be borne in mind in order to understand what kind of phenomena can be explained by the model and what effects lie outside this description.

3.1 Basic assumptions of the MHD model

The MHD model regards the plasma as a quasi-neutral electrically conducting fluid. The first and most fundamental assumption of this description is to regard the ensemble of ions and electrons conforming the plasma as a single continuum medium. This is valid when the length scales associated with the magnetic field gradients is much larger than the internal length scales of the plasma (such as the ionic and electronic gyroradii). This condition holds in virtually every laboratory plasma dedicated to fusion research.

The second important assumption is to consider that the plasma is in thermodynamic equilibrium so the particles have a Maxwellian distribution of velocities. This is a good approximation as long as the shortest time scale of the process under consideration is much longer than the collision time and the shortest length scale of the system is larger than the mean free path of the particles. In other words, the plasma should be in a collisional regime (this condition is required to derive the fluid equations from the kinetic equations (Braginskii, 1965)). The collisionality hypothesis is usually not satisfied at the highest temperatures obtained in modern tokamak experiments. However, spheromak plasmas are much colder ($T \sim 10^2$ eV) so that this assumption is still reasonable. Moreover, there are several arguments supporting the validity of the MHD model even in collisionless systems (Friedberg, 1987); (Priest & Forbes, 2000).

Finally, in the context of the MHD model the plasma is assumed to be electrically neutral (or quasi-neutral since the charges are present but exactly balanced). This is approximately true when the length scales under consideration are larger than the Debye shielding of electrons.

3.2 MHD equations

Now we seek for the equations that describe the evolution of the two main quantities that govern the dynamics of such an MHD system: the velocity field and the magnetic field. The equation for the evolution of the plasma velocity $\mathbf{u}$, expresses the balance of linear momentum

$$\rho\left(\frac{\partial \mathbf{u}}{\partial t} + \mathbf{u}\cdot\nabla\mathbf{u}\right) = -\nabla p + \mathbf{J}\times\mathbf{B} + \mu\nabla\cdot\Pi \tag{7}$$

where ρ is the mass density and p is the thermodynamic pressure. The second term on the right hand side is the Lorentz force, where $\mathbf{J}$ is the current density and $\mathbf{B}$ is the magnetic field. We note that due to quasi-neutrality the current density is produced by the relative motion

between ions and electrons. The last term in Eq. (7) is the viscous force where $\mu = \rho\nu$ is the dynamic viscosity, ν is the cinematic viscosity and the tensor Π is given by

$$\Pi = \nabla\mathbf{u} + \nabla\mathbf{u}^T - \frac{2}{3}(\nabla \cdot \mathbf{u})\mathbf{I}. \tag{8}$$

If the flow is incompressible ($\nabla \cdot \mathbf{u} = 0$) Π reduces to $\nabla\mathbf{u}$.

Let us mention some basic aspects of the Lorentz force term. Using the low-frequency Ampère law $\mathbf{J} = \nabla \times \mathbf{B}$ (we rescale $\mathbf{B}$ and $\mathbf{J}$ in such a way that $\mu_0 = 1$) and the vector identity $(\nabla \times \mathbf{B}) \times \mathbf{B} = (\mathbf{B} \cdot \nabla)\mathbf{B} - \nabla(B^2/2)$, we can decompose this term into two contributions

$$\mathbf{J} \times \mathbf{B} = (\mathbf{B} \cdot \nabla)\mathbf{B} - \nabla\left(\frac{B^2}{2}\right). \tag{9}$$

The first term on the right represents a magnetic tension force in the direction of $\mathbf{B}$ which has a restoring effect when the magnetic field lines are bent. The second term is regarded as a magnetic pressure that acts in all directions. Clearly, both forces must cancel out along the magnetic field lines since the term $\mathbf{J} \times \mathbf{B}$ can not accelerate the fluid in the direction of $\mathbf{B}$.

The equation for the magnetic field evolution comes from the Maxwell equations and a constitutive law that relates the electric field to the magnetic field and the current density (the Ohm's law). We begin with the Faraday's law in the low-frequency limit (i.e. neglecting the displacement current)

$$\nabla \times \mathbf{E} = -\frac{\partial \mathbf{B}}{\partial t}. \tag{10}$$

On the other hand, the Ohm's law relates the current density to the electric field in the frame of reference of the conducting medium $\mathbf{E}' = \eta\mathbf{J}'$, where η is the electric resistivity (the reciprocal of the conductivity) and the prime denotes that the quantities have to be measured in the plasma's reference frame. When this equation is expressed in the lab's frame (from which the plasma moves at velocity $\mathbf{u}$) it adopts the form

$$\mathbf{E} = -\mathbf{u} \times \mathbf{B} + \eta\mathbf{J} \tag{11}$$

where relativistic effects have been neglected ($u \ll c$, where c is the speed of light).

Combining Eqs. (10) and (11) together with the identity $\nabla \times \nabla \times \mathbf{B} = \nabla(\nabla \cdot \mathbf{B}) - \nabla^2\mathbf{B}$ and the constraint $\nabla \cdot \mathbf{B} = 0$, we obtain the MHD induction equation

$$\frac{\partial \mathbf{B}}{\partial t} = \nabla \times (\mathbf{u} \times \mathbf{B}) + \eta\nabla^2\mathbf{B} \tag{12}$$

where spatial uniformity of η was assumed. Although not considered in this work, we point out that, whenever present, resistivity gradients may give rise to the so-called current interchange effect which constitutes an effective mechanism of current exchange between flux tubes (Zheng & Furukawa, 2010). Note that the terms $\mathbf{J} \times \mathbf{B}$ and $\mathbf{u} \times \mathbf{B}$ introduce a strong non-linear coupling between Eqs. (7) and (12).

3.3 Diffusion of magnetic field lines and frozen-in-flux condition

The two terms in the right hand side of Eq. (12) account for two very different physical effects. The quotient between the magnitudes of these effects can be estimated as

$$\frac{|\nabla \times (\mathbf{u} \times \mathbf{B})|}{|\eta \nabla^2 \mathbf{B}|} \sim \frac{u_0/L}{\eta/L^2} = \frac{u_0 L}{\eta} \equiv R_m \tag{13}$$

where u_0 and L are typical velocity and length scales and R_m is the magnetic Reynolds number. Thus, when $R_m \sim 0$ the magnetic field simply diffuses and the configuration decays in the resistive time scale $\tau_r = L^2/\eta$.

The opposite limit ($R_m \gg 1$) is more representative of the actual situation in most laboratory (in the context of magnetic confinement) and space plasmas. In this limit (called ideal limit) the induction equation reduces to,

$$\frac{\partial B}{\partial t} = \nabla \times (\mathbf{u} \times \mathbf{B}) \qquad (R_m \gg 1). \tag{14}$$

This equation implies the conservation of the magnetic flux through any closed surface that moves with the local velocity of the fluid. If we regard the magnetic field lines as very thin flux tubes and we imagine closed curves surrounding them that move with the fluid, we realize that the plasma drags the field lines as it moves. It is said that the field lines are frozen in the plasma (*frozen-in-flux condition*). Since each field line is simply convected by the flow (assumed to be smooth and continuous) its connectivity is preserved. This means that in the ideal MHD approximation the changes in the topology of the magnetic field are not possible. This idea, which is intimately related to the Kelvin's circulation theorem for inviscid flows, was first introduced by Hannes Alfvén in 1943. More details on the frozen in flux condition may be found elsewhere (Biskamp, 2000);(Priest & Forbes, 2000).

3.4 Closing the system of equations

The system formed by Eqs. (7) and (12) and the constraint $\nabla \cdot \mathbf{B} = 0$, has too many unknowns and can not be solved. Even if the current density can easily be expressed in terms of the magnetic field using Ampère's law, we still need to introduce some information concerning the density and the pressure. We describe four common approaches to accomplish this.

Firstly, the zero-β approximation gives the simplest option. The nondimensional parameter $\beta = 2p_0/B_0^2$ measures the ratio between the thermodynamic pressure and the magnetic pressure. A very low β value (which is the case in most confinement experiments) means that the dynamics of the plasma is mainly dictated by the magnetic field (via the Lorentz force) while the pressure gradient has little influence. Thus, we may simply remove the term ∇p from Eq. (7) and assume that $\rho = \rho_0$ is a constant.

The second option is to consider an incompressible flow. In this case ρ is still a constant but the pressure gradient is no dropped. In this case the required information is completed by the incompressible condition $\nabla \cdot \mathbf{u} = 0$. The pressure can not be directly computed with this equation but it can be indirectly inferred. It plays the role of a Lagrange multiplier. Although this is a less crude and more consistent option, it is not generally a good approximation for low β plasmas.

Thirdly, we could allow compressible flows by using the continuity equation

$$\frac{\partial \rho}{\partial t} + \nabla \cdot (\rho \mathbf{u}) = 0 \tag{15}$$

and assuming some simple relationship between the pressure and the density. For instance, $p = c_s^2 \rho$ where c_s is the speed of sound (isothermal approximation) or $p = c_{ad} \rho^\gamma$ where c_{ad} is a constant and γ is the polytropic index (polytropic approximation).

Finally, a more elaborated option can be obtained if we incorporate, besides Eq. (15), an equation for the energy balance

$$\frac{\partial w}{\partial t} = -\nabla \cdot \mathbf{q} - Q_{c,r} \tag{16}$$

where w is the total energy density defined as

$$w = \rho \left(\frac{u^2}{2} + e \right) + \frac{B^2}{2} \tag{17}$$

e is the internal energy per unit of mass, the term $Q_{c,r}$ accounts for conductive and radiative losses and $\mathbf{q}$ is the energy flux given by

$$\mathbf{q} = \left[\rho \left(e + \frac{u^2}{2} \right) + p \right] \mathbf{u} + \mathbf{E} \times \mathbf{B} - \mu (\mathbf{u} \cdot \Pi). \tag{18}$$

The three terms on the right denote respectively the energy flux due to convection, the electromagnetic energy flux (Poynting's vector) and the viscous dissipation of energy. In this context we also need an equation of state of the form $p = p(\rho, e)$. The most common choice is the ideal gas law $p = (\gamma - 1)\rho e$ where γ is the ratio of specific heats.

3.5 Scales and dimensionless numbers

The results presented in Sec. 5 are obtained by numerically solving the MHD equations. It is a common practice to use a nondimensionalized version of the considered equations. The removal of the units is achieved by the choice of suitable scales that can be condensed in few nondimensional numbers. We will see which are the chosen scales and the relevant nondimensional quantities in this study.

Since spheromaks are very low-β plasmas, the zero-β approximation is used to close the system. The resulting equations can be nondimensionalized with a length scale a (the radius of the cylinder inside which we will solve the equations) and a velocity scale $c_A = B/\sqrt{\rho}$, which is known as the Alfvén velocity. Perpendicular perturbations travel along the magnetic field lines at this velocity. The time will be normalized by the Alfvén time $\tau_A = a/c_A$, which represents the typical time scale of the MHD fluctuations.

Using these scales we obtain two nondimensional numbers: the Lundquist number $S = ac_A/\eta$ and ν/ac_A which is usually expressed in terms of the magnetic Prandtl $P_m = \nu/\eta$. The Lundquist number can be rewritten as

$$S = \frac{a^2/\eta}{a/c_A} = \frac{\tau_r}{\tau_A} \tag{19}$$

where τ_r is the time scale of resistive dissipation. In the simulations presented in Sec. 5 we have used $P_m = 1$ and $S = 2 \times 10^4$.

4. Plasma relaxation

It is common to observe magnetized fluids and plasmas as well as other continuum media to exist naturally in states with some kind of large scale order. These states are to some extend independent of the initial conditions, that is to say, they are preferred configurations toward which the system evolves if the correct boundary conditions are imposed. Moreover, if the system is perturbed it tends to return to the same preferred state recovering the large scale order. The large scale order of some quantity always comes together with the disorder at small scales of another quantity. These preferred configurations are called *self-organized* sates and the dynamical process of achieving these states is called *self-organization* (Hasegawa, 1985). Plasma relaxation is an example of self-organization.

Self-organized (or relaxed) states can not be deduced from force balance or stability considerations alone. The theory of magnetic relaxation always relies on some variational principle, that is to say, the minimization of some quantity subjected to one or more constraints. Possibly the simplest and surely the most widespread option adopted to describe plasma relaxation was introduced by Taylor (1974). While a rather obvious choice was made for the quantity to minimize (the magnetic energy) a very clever option was made for the constraint. Among all the ideal MHD invariants Taylor chose the total magnetic helicity. The total magnetic helicity quantifies several topological properties of the system and even when magnetic reconnection can change the topology of the magnetic field lines, the total helicity of the system is still a robust invariant. These ideas are further developed below.

4.1 Magnetic helicity

The total magnetic helicity H of the magnetic field $\mathbf{B}$ within the volume V is

$$H = \int_V \mathbf{A} \cdot \mathbf{B} \, dV \tag{20}$$

where $\mathbf{A}$ is the potential vector ($\mathbf{B} = \nabla \times \mathbf{A}$). A relevant question may be posed at this time regarding how this quantity is modified by a change in the gauge of $\mathbf{A}$. It is clear that in order to have a meaningful definition, Eq. (20) should be gauge invariant. The helicity change ΔH introduced when $\mathbf{A}$ is replaced by $\mathbf{A} + \nabla\chi$ is

$$\Delta H = \int_V \nabla\chi \cdot \mathbf{B} \, dV = \int_V \nabla \cdot (\chi \mathbf{B}) \, dV \tag{21}$$

where we have used the fact that $\nabla \cdot \mathbf{B} = 0$. Applying the divergence theorem in a simply connected volume V this becomes

$$\Delta H = \int_S \chi \mathbf{B} \cdot \mathbf{ds} \tag{22}$$

where S is the surface that encloses V and $\mathbf{ds}$ is the outward-pointing normal surface element. Therefore, the definition (20) is gauge invariant only if the normal component of the magnetic field vanishes at the boundary of V, which was assumed to be simply connected. We will

respect these two conditions throughout this work. When the normal component of the magnetic field does not vanish at the boundary or the volume V is not simply connected a generalized definition, the so-called *relative helicity*, must be employed (Finn & Antonsen, 1985).

To see how H can measure topological properties of the system we will consider the concept of flux tube. The magnetic flux through an open and orientable surface S is

$$\Phi = \int_S \mathbf{B} \cdot \mathbf{ds} = \oint_C \mathbf{A} \cdot \mathbf{dl} \tag{23}$$

where C is the path along the perimeter of S in the counterclockwise direction. Note that the Eq. (23) holds even if the gauge of $\mathbf{A}$ is changed.

We present an example given by Moffat (1978). Consider two linked flux tubes like those shown in Fig. 2 (a). We assume that there are no other contributions to the magnetic field. In

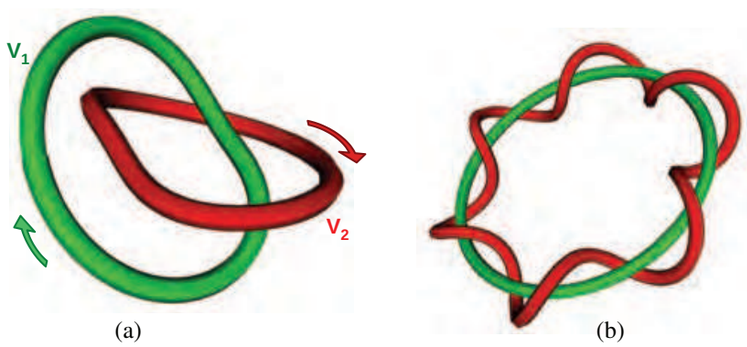

(a) (b)

Fig. 2. Linked flux tubes.

this simplified case the total helicity can be computed as $H = H_1 + H_2$, with $H_i = \int_{V_i} \mathbf{A} \cdot \mathbf{B}\, dV$, for $i = 1, 2$. To compute H_i we note that $dV = \mathbf{dl} \cdot \mathbf{ds}$, where $\mathbf{dl}$ is the element of length along the tube and $\mathbf{ds}$ its cross section. By construction, $\mathbf{dl}$ and $\mathbf{ds}$ are parallel to $\mathbf{B}$, so we can rearrange the integrand as $\mathbf{A} \cdot \mathbf{B}\, dV = \mathbf{A} \cdot \mathbf{B}\, \mathbf{dl} \cdot \mathbf{ds} = (\mathbf{A} \cdot \mathbf{dl})(\mathbf{B} \cdot \mathbf{ds})$, and thus

$$H_i = \oint_{C_i} \int_{S_i} (\mathbf{A} \cdot \mathbf{dl})(\mathbf{B} \cdot \mathbf{ds}). \tag{24}$$

Since the magnetic flux is constant along each curve C_i the last equation can be written as

$$H_i = \Phi_i \oint_{C_i} \mathbf{A} \cdot \mathbf{dl}. \tag{25}$$

On the other hand, the contour C_1 encloses the magnetic flux Φ_2 and vice versa, so from Eq. (23) it is clear that

$$\oint_{C_1} \mathbf{A} \cdot \mathbf{dl} = \Phi_2 \qquad \text{and} \qquad \oint_{C_2} \mathbf{A} \cdot \mathbf{dl} = \Phi_1 \tag{26}$$

and thus $H_1 = H_2 = \Phi_1 \Phi_2$ which finally gives

$$H_{\text{link}} = 2\Phi_1 \Phi_2 \tag{27}$$

for the helicity due to the linking of the tubes. In general, if each tube winds around the other N times (in Fig. 2 (b) we have $N = 6$) one obtains $H_1 = H_2 = N\Phi_1\Phi_2$ (Moffat, 1978). N is the *linking number* of the tubes.

The helicity can also measure the self-twisting of a single tube. So far we did not pay attention to the tube's cross section shape. In order to compute the helicity of a twisted flux tube it is convenient to consider structures having elongated cross sections, like the ribbon shown in Fig. 3 (a). This ribbon is untwisted and has no helicity. If we cut this ribbon, we rotate one end

Fig. 3. (a) An untwisted ribbon-like flux tube, (b) a twisted flux tube and (c) the same twisted tube marked with different colors.

by 2π and we join both ends together again we obtain the twisted ribbon shown in Fig. 3 (b). The helicity of this structure may be computed using Eq. (27) obtained for two linked tubes applying the following reasoning. Regard the twisted tube as two adjacent tubes carrying one half of the total magnetic flux (see Fig. 3 (c)). The helicity of this system has a contribution coming from the linking of the two tubes H^1_{link} and also a contribution coming from the self twisting of the smaller tubes. If Φ is the total magnetic flux of the original twisted tube, the helicity due to the linking of each half is

$$H^1_{\text{link}} = 2\left(\frac{\Phi}{2}\right)^2. \tag{28}$$

Note that this mental process to convert helicity due to twisting into helicity due to linking can be recursively applied to obtain

$$H^n_{\text{link}} = 2^n\left(\frac{\Phi}{2^n}\right)^2 = \frac{\Phi^2}{2^n} \tag{29}$$

for each contribution due to linking. Finally, the helicity of the twisted tube is obtained by adding all these contributions

$$H = \lim_{N\to\infty}\sum_{n=1}^{N} H^n_{\text{link}} = \Phi^2\sum_{n=1}^{\infty}\frac{1}{2^n} = \Phi^2. \tag{30}$$

4.2 Localized magnetic reconnection

Magnetic reconnection is ubiquitous in almost all space and laboratory plasmas. It consists in a rearrangement of the topology of the magnetic field due to a change in the connectivity of the magnetic field lines. This process plays an important role in several confinement devices (such us the tokamak, the RFP and the spheromak) as well as in several astrophysical phenomena (Earth magnetosphere, solar corona, solar wind, accretion disks, etc.). Since the majority of those plasmas have a very high magnetic Reynolds number (and a high Lundquist number as well) the ideal MHD model should provide an adequate level of description for the physical system. However, as already mentioned in Sec. 3.3, topological changes in the magnetic field are not allowed in the ideal limit. What actually happens is that the coupled non linear evolution of the magnetic field and the flow inevitably develops *current sheets*, i.e. localized regions where the magnetic field gradients become very large. Within these highly localized regions the ideal approximation breaks down and the last term of Eq. (12) becomes relevant causing the magnetic field to diffuse and change the connectivity of the field lines.

The fundamental *ansatz* of the plasma relaxation theory is that these localized reconnection events do not change the total helicity of the system. Even when dissipation is involved in this process, it is assumed that only magnetic energy is affected. How can magnetic helicity be conserved during a localized reconnection event is schematically shown in Fig. 4. Two

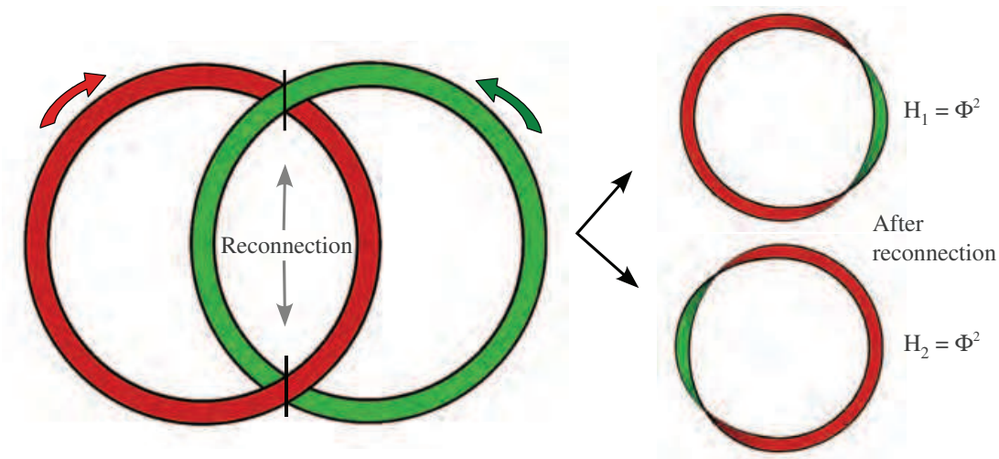

Fig. 4. (a) Two linked ribbon-like flux tubes undergo a localized reconnection process that give rise to two separate but twisted tubes (b). The global helicity of the system is conserved.

untwisted flux tubes that are initially linked can be locally reconnected giving rise to a pair of separate but twisted tubes, in such a way that the total helicity of the system is conserved.

Moreover, plasma relaxation is based on the fact that localized reconnection events allow topological changes and dissipate magnetic energy much faster than the total helicity. There exists a number of arguments to justify this behavior (see Sec. 9.1.1 of Priest & Forbes (2000) or Montgomery et al. (1978)). Let's consider, for instance, how these two quantities (magnetic energy and helicity) decay in the presence of a small uniform resistivity η. Magnetic energy,

$W = \int_V B^2/2\, dV$, decays at the rate

$$\frac{dW}{dt} = -\eta \int_V J^2\, dV. \tag{31}$$

This expression can be obtained by scalar multiplying Eq. (10) by $\mathbf{B}$ and integrating over a fixed volume at whose boundary the normal component of the Poynting vector vanishes. For the magnetic helicity we take the time derivative of (20) and obtain

$$\frac{dH}{dt} = \int_V \left(\frac{\partial \mathbf{A}}{\partial t} \cdot \mathbf{B} + \mathbf{A} \cdot \frac{\partial \mathbf{B}}{\partial t} \right) dV = \int_V \left(\frac{\partial \mathbf{A}}{\partial t} \cdot \mathbf{B} + \mathbf{A} \cdot \nabla \times \frac{\partial \mathbf{A}}{\partial t} \right) dV. \tag{32}$$

Using vector identities and the divergence theorem, the last expression can be rewritten as

$$\frac{dH}{dt} = 2 \int_V \frac{\partial \mathbf{A}}{\partial t} \cdot \mathbf{B}\, dV - \int_S \mathbf{A} \times \frac{\partial \mathbf{A}}{\partial t} \cdot \mathbf{ds} \tag{33}$$

where S is the surface that encloses V. If field lines do not penetrate the volume V the surface integral in Eq. (33) vanishes. In the absence of charge separation $\mathbf{E} = -\partial \mathbf{A}/\partial t$, and using Ohm's law $\mathbf{E} = \eta \mathbf{J}$, we finally obtain

$$\frac{dH}{dt} = -2\eta \int_V \mathbf{J} \cdot \mathbf{B}\, dV. \tag{34}$$

It is clear that in the absence of resistivity (the ideal limit) W and H are conserved and, for this reason, it is said that they are ideal invariants. By contrast, in a real plasma both energy and helicity will decay at a rate proportional to η. However, when turbulence is present, magnetic fluctuations produce many thin current sheets with thicknesses of order $\eta^{1/2}$ and current densities proportional to $B\eta^{-1/2}$. In such case, the energy decay rate becomes

$$\frac{dW}{dt} \propto \int_V B^2\, dV$$

which is independent of η. On the other hand, the total helicity decays as

$$\frac{dH}{dt} \propto 2\eta^{1/2} \int_V B^2 dV$$

so that as η tends to zero the helicity dissipation becomes negligible. Therefore, it is important to keep in mind that a plasma will relax (in the sense described here) only if there is a certain level of small scale fluctuations that gives rise to many localized current sheets. For this reason, relaxation theory does not apply to devices with a very low level of magnetic fluctuations, such as the tokamak.

Localized magnetic reconnection events may redistribute currents in the plasma by helicity transfer between flux tubes. Even when this idea must be applied with care because the helicity is by definition a global quantity, it is clear that the helicity of a single flux tube may change after reconnection with another flux tube. This helicity transfer process is certainly at work during toroidal current drive in spheromaks and other devices sustained by helicity injection.

4.3 Relaxed states

The magnetic relaxation theory is developed for systems in which the magnetic forces are dominant, i.e. whenever the parameter β is low. In such cases, the MHD equilibrium Eq. (1) reduces to the force-free condition

$$\nabla \times \mathbf{B} = \lambda(\mathbf{r})\, \mathbf{B} \tag{35}$$

where $\lambda(\mathbf{r})$ is some scalar function. As discussed in the previous Section, magnetic fluctuations induce localized reconnection events that relax the plasma toward the state of minimum magnetic energy maintaining the total helicity of the system (Taylor, 1974). Woltjer (1958) has shown that force-free fields with λ equal to a constant represent the state of lowest magnetic energy under the constraint of magnetic helicity conservation in a closed system (i.e. with no field lines intercepting the boundary). The proof uses the method of Lagrange multipliers. At a constrained minimum, the variation of magnetic energy is equal to a constant (the Lagrange multiplier) times the variation of helicity

$$\delta W = \frac{\lambda}{2} \delta H \tag{36}$$

where $\lambda/2$ is the Lagrange multiplier. Substituting $W = \int_V B^2/2\, dV$ for the magnetic energy and Eq. (20) for H yields

$$\int_V \left[2\, \mathbf{B} \cdot \delta\mathbf{B} - \lambda(\delta\mathbf{A} \cdot \mathbf{B} + \mathbf{A} \cdot \delta\mathbf{B}) \right] dV = 0. \tag{37}$$

Using the identities

$$\mathbf{B} \cdot \delta\mathbf{B} = \delta\mathbf{A} \cdot \nabla \times \mathbf{B} - \nabla \cdot (\mathbf{B} \times \delta\mathbf{A})$$

and

$$\mathbf{A} \cdot \delta\mathbf{B} = \mathbf{B} \cdot \delta\mathbf{A} + \nabla \cdot (\delta\mathbf{A} \times \mathbf{A})$$

and the divergence theorem in Eq. (37) one obtains

$$\int_V 2\, (\nabla \times \mathbf{B} - \lambda\mathbf{B}) \cdot \delta\mathbf{A}\, d^3r = 0 \tag{38}$$

where we omitted the surface integrals because they vanish in the absence of field lines penetrating the volume under consideration. Since $\delta\mathbf{A}$ is arbitrary, the parenthesis of the integrand of Eq. (38) must be identically zero, which finally gives us the linear force-free condition

$$\nabla \times \mathbf{B} = \lambda\mathbf{B} \tag{39}$$

where λ is a constant. When we impose $\mathbf{B} \cdot \mathbf{ds} = 0$ at the boundary, we obtain an eigenvalue problem that has non trivial solution only for certain discrete values λ_n (which are real and positive).

Since $\nabla \times \mathbf{B} = \lambda_n \mathbf{B}$, we can write the magnetic field as $\mathbf{B} = \lambda_n \mathbf{A} + \nabla f$, where f is an arbitrary potential. Thus, we can compute the magnetic energy as

$$W = \frac{1}{2} \int_V \mathbf{B} \cdot (\lambda_n \mathbf{A} + \nabla f) dV = \frac{\lambda_n}{2} \int_V \mathbf{B} \cdot \mathbf{A}\, dV = \frac{\lambda_n}{2} H \tag{40}$$

since $\int_V \mathbf{B} \cdot \nabla f dV = \int_V \nabla \cdot (f\mathbf{B}) dV = \int_{\partial V} (f\mathbf{B}) \cdot \mathbf{ds} = 0$. Eq. (40) gives us an important meaning for the eigenvalue: λ_n is proportional to the quotient W/H. For this reason it is clear that for a given amount of helicity, the minimum energy state will be given by the lowest allowed value of λ_n (i.e. λ_1).

The most frequent model employed to describe a spheromak configuration is the relaxed state inside a cylindrical flux conserver. Using cylindrical coordinates, the condition $\mathbf{B} \cdot \mathbf{ds} = 0$ means $B_z = 0$ at $z = 0$ and $z = h$ and $B_r = 0$ at $r = a$, where h and a are the height and the radius of the cylinder. In this case the solution to Eq. (39) can be found analytically (Bellan, 2000). In terms of Bessel functions and trigonometric functions the solution is

$$B_r = B_0 \frac{\pi}{\gamma_1 h} J_1(\gamma_1 r) \cos(k_1(z-h)) \tag{41}$$

$$B_\theta = -B_0 \frac{\lambda_1}{\gamma_1} J_1(\gamma_1 r) \sin(k_1(z-h)) \tag{42}$$

$$B_z = -B_0 J_0(\gamma_1 r) \sin(k_1(z-h)) \tag{43}$$

where $\gamma_1 = x_{11}/a$, $k_1 = \pi/h$ and x_{11} is the first zero of J_1. Note that, since this is an eigenfunction (of the curl operator) it is defined up to a constant B_0. Note also that this solution has no toroidal dependence (i.e. it is axisymmetric). The corresponding eigenvalue which depends on the geometry of the flux conserver is

$$\lambda_1 = \sqrt{\frac{x_{11}^2}{a^2} + \frac{\pi^2}{h^2}}. \tag{44}$$

In Fig. 5 we show the magnetic field lines obtained after following the trajectories given by Eqs. (41) - (43) from four different positions.

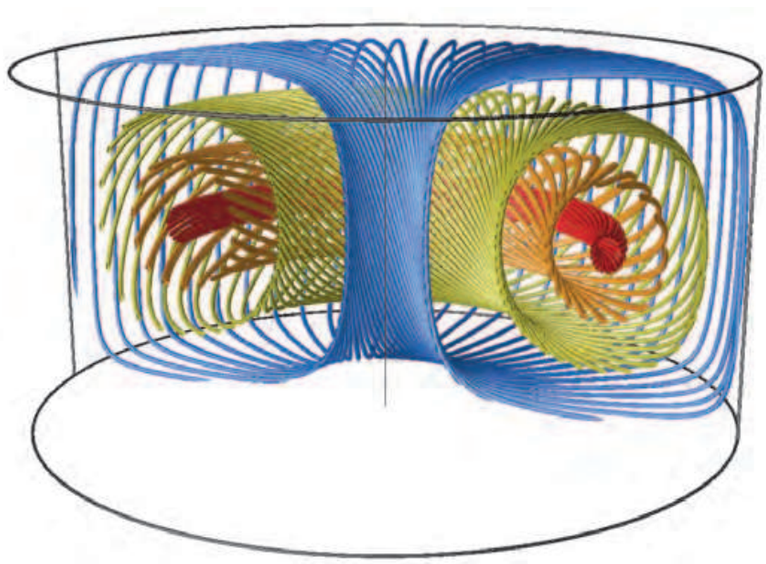

Fig. 5. Four magnetic field lines showing four nested magnetic flux surfaces. This fully relaxed state has the same value of λ (equal to λ_1) on each surface.

5. Dynamics of magnetic relaxation in spheromak configurations

The relaxation theory as formulated by Taylor (1974) is a variational principle that can not give details on the dynamical aspects of the process. All the considerations we have made regarding the important role of localized reconnection in helicity conservation are only heuristic arguments that try to explain the remarkable success of the theory at predicting the self-organized final state of the plasma.

There are a number of reasons that motivate the study of the dynamics of relaxation. For instance, in the context of spheromak research it is observed that during sustainment the system does not remain at the lowest energy state. Small deviations from the relaxed state as well as the ubiquitous presence of fluctuations are crucial issues that are out of the scope of relaxation theory (Knox et al., 1986);(Willet et al., 1999). In this work we study these aspects using numerical solutions of the non linear resistive MHD equations described in Sec. 3 as an initial and boundary value problem in three spatial dimensions. The nondimensional version described in Sec. 3.5 of these equations is used. The details of the numerical method are not presented here but can be found elsewhere (Garcia-Martinez & Farengo, 2009b).

In this Section we present a study of the dynamics of the kink mode in spheromak configurations. We will focus on the dynamics of systems that are only marginally unstable. Even when this may sound as a rather specific topic we will see that this is a simple setup in which we can study magnetic reconnection and helicity transfer between flux tubes. Firstly, we describe the kink unstable configurations used as initial condition and explain how they can be computed. Secondly, we study the dynamics of the kink instability in several cases and discuss in which cases it leads to a complete relaxation process (as described in the preceding Section) and in which cases the relaxation process is only partial. Thirdly, we introduce the concept of safety factor and resonant surfaces and explain their relevance to the partial relaxation behavior observed in marginally unstable configurations. Then, we analyze in detail the reconnection process that is driven by the dominant kink mode. Finally, we discuss simple models to describe this reconnection process.

5.1 Problem description

The minimum energy state for a given helicity inside a (not very elongated) cylindrical flux conserver, see Fig. 5, is stable against small MHD perturbations. There exists, however, a simple modification of this configuration which is MHD unstable, in particular *kink* unstable. Now we derive the equations that will allow us to compute as well as to better understand these modified configurations.

For simplicity we consider force-free configurations. In general this condition may be expressed as $\mathbf{J} = \lambda(\mathbf{r})\mathbf{B}$, where λ may be an arbitrary function. However, we will restrict our study to the case in which λ is a flux function, that is to say it takes the same value on each flux surface and can only change from one surface to another. This condition is expressed as

$$\nabla \times \mathbf{B} = \lambda(\psi)\mathbf{B}. \tag{45}$$

Since we consider axisymmetric configurations, we can express the poloidal magnetic field component ($\mathbf{B}_p$) in terms of ψ using Eq. (4), while for the toroidal component we have

$$J_z = (\nabla \times \mathbf{B})_z = \frac{1}{r}\frac{\partial}{\partial r}(rB_\theta) = \lambda B_z. \tag{46}$$

Using this, along with Eq. (3) we obtain

$$B_\theta = \frac{1}{2\pi r}\int_0^r \lambda B_z \, 2\pi\tilde{r}d\tilde{r} = \frac{1}{2\pi r}\int_0^\psi \lambda(\tilde{\psi})d\tilde{\psi}. \tag{47}$$

Thus, expressing the magnetic field in terms of ψ we can rewrite the toroidal component of Eq. (45) as

$$\frac{\partial^2\psi}{\partial r^2} - \frac{1}{r}\frac{\partial\psi}{\partial r} + \frac{\partial^2\psi}{\partial z^2} + \lambda(\psi)\int_0^\psi \lambda(\tilde{\psi})d\tilde{\psi} = 0 \tag{48}$$

which is the force-free version of the Grad-Shafranov equation. We are interested in solving Eq. (48) in the rectangle $\Omega : (r,z) = [0,a]\times[0,h]$, i.e. a cylinder of radius a and height h.

The most simple option for $\lambda(\psi)$ would be $\lambda = 0$, which corresponds to the vacuum solution (currentless magnetic field). The solution vanishes in this case if homogeneous boundary conditions ($\psi|_{\partial\Omega} = 0$) are applied.

A more interesting case is obtained by setting $\lambda = \lambda_n$ (constant) which gives

$$-\Delta^*\psi = \lambda_n^2\psi \tag{49}$$

where we have introduced the Grad-Shafranov operator defined as $\Delta^* = \partial^2/\partial r^2 - (1/r)\partial/\partial r + \partial^2/\partial z^2$. If we impose homogeneous boundary conditions we obtain an eigenvalue problem which has non trivial solutions only for a discrete set of real and positive values of λ_n. The lowest value (λ_1) is given by Eq. (44) and its associated eigenfunction is the minimum energy state described in detail in Sec. 4.3. Thus, if the appropriate boundary conditions are imposed, we can also regard the spheromak as the lowest eigenfunction of the Grad-Shafranov operator.

In this study we will consider initial equilibria having

$$\lambda(\psi) = \bar{\lambda}\left[1 + \alpha\left(2\frac{\psi}{\psi_{ma}} - 1\right)\right] \tag{50}$$

which is a linear $\lambda(\psi)$ profile with slope α and mean value $\bar{\lambda}$. When this linear profile is injected in Eq. (48) a generalized non-linear eigenvalue problem is obtained. Some mathematical considerations as well as a basic numerical scheme to solve this problem were given by Kitson & Browning (1990). Note that even if one is able to solve the non-linear Grad-Shafranov equation, the profile given by Eq. (50) includes ψ_{ma} which is not know *a priori*. The procedure adopted here is to set $\psi_{ma} = 1$, fix the desired value of α and iterate over $\bar{\lambda}$ until ψ is equal to one at the magnetic axis. With this procedure we obtain the values of $\bar{\lambda}$ listed in Table 1. Note that each α value uniquely defines a configuration.

In Fig. 6 (a) we show two linear $\lambda(\psi)$ profiles and (b) ψ contours and the λ colormap for the $\alpha = -0.4$ case. The reason why we have chosen negative values for α is the following. It is evident that for negative values of the slope the configuration will have larger λ values in the outer flux surfaces (at lower ψ values) and *vice versa*. Since λ is proportional to the current

α	0	-0.3	-0.4	-0.5	-0.6	-0.7	-0.8
$\bar{\lambda}$	4.95	5.08	5.18	5.32	5.51	5.78	6.23

Table 1. $\bar{\lambda}$ values for some prescribed α values.

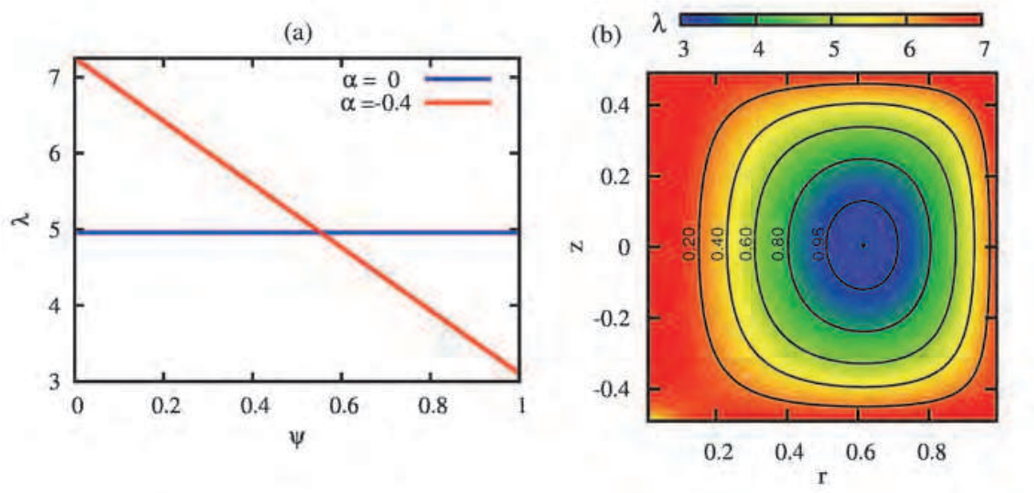

Fig. 6. (a) Two $\lambda(\psi)$ profiles. (b) ψ contours and λ colormap for the case with $\alpha = -0.4$. A hollow current profile is obtained for negative α values.

density it is said that the configuration has a *hollow* current profile. This is actually the case for spheromak configurations during sustainment.

Real spheromaks have some amount of open magnetic surfaces (i. e. there is some magnetic flux crossing the walls) along which current is driven. This injects magnetic helicity. Then the system relies on magnetic relaxation to drive the current in the inner flux surfaces. In order to sustain this current drive process in (quasi) steady state, some current (or λ) gradient is required. In fact, experiments show that sustained spheromaks are better approximated by a force-free state with $\alpha = -0.3$ rather than by the lowest energy state (having $\alpha = 0$) (Knox et al., 1986); (Willet et al., 1999).

5.2 Complete relaxation vs partial relaxation

Up to this point we know that the minimum energy state is MHD stable and that we can modify the configuration by giving the $\lambda(\psi)$ profile a non zero slope. Now we consider the stability of configurations having negative α values. A linear MHD stability analysis has determined that there exists a threshold value for the slope at which the system becomes unstable (Knox et al., 1986). Configurations with $\lambda(\psi)$ profiles that are steeper than the threshold (lower α values) are unstable while configurations with less steep profiles are stable. The value of this threshold (which lies between -0.3 and -0.4 for the geometry used here) was also verified using non-linear simulations of spheromak configurations (Garcia-Martinez & Farengo, 2009b).

The instability that arises has dominant toroidal number $n = 1$ (where n stands for the number of the coefficient of the Fourier decomposition in the toroidal direction). This current driven $n = 1$ mode is the kink mode. It is well known that the kink mode triggers the relaxation process in spheromaks during sustainment. It has been shown that when the initial unstable configuration has an α value close to the stability threshold, the relaxation process is not complete (Garcia-Martinez & Farengo, 2009a);(Garcia-Martinez & Farengo, 2009b). This means that the final state of the evolution is not a minimum energy state. In particular, the λ profile is not uniform. This partial relaxation behavior can be observed in Fig. 7. In the

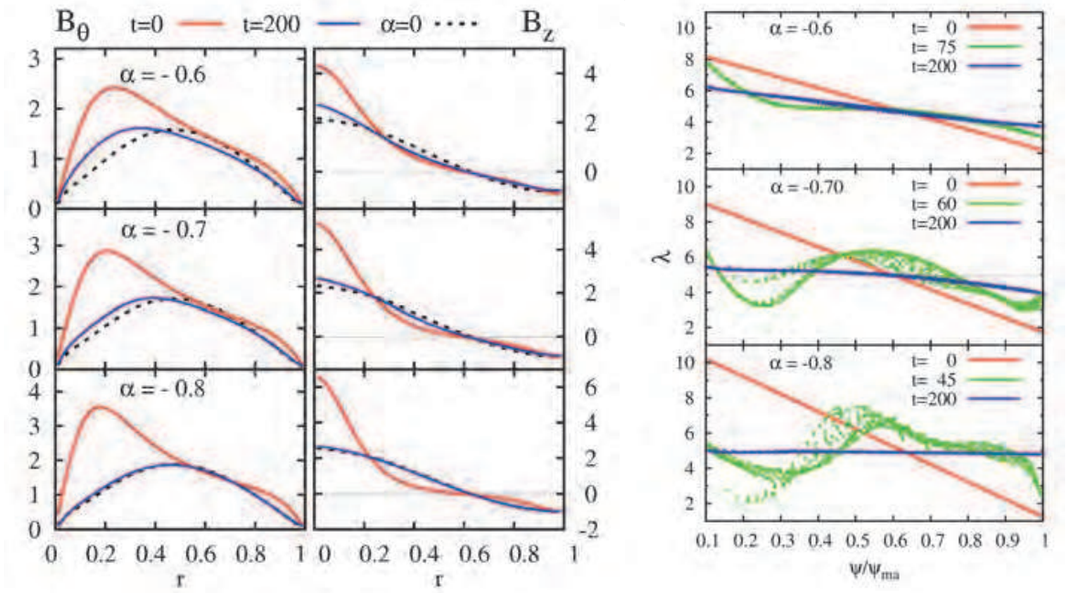

(a) (b)

Fig. 7. (a) Toroidal and poloidal magnetic field profiles at $t = 0$ and $t = 200$ (final time). The dashed line shows the fully relaxed profiles. (b) $\lambda(\psi)$ profiles at three times for the same α values (Garcia-Martinez & Farengo, 2009b).

$\alpha = -0.6$ case it is clear that the final state does not have neither the same radial magnetic field profiles than the minimum energy state (shown in dashed lines) nor a uniform λ profile. On the other hand, the most unstable case, $\alpha = -0.8$, exhibits a fully relaxed final state.

Fig. 8 shows the evolution of the magnetic field lines during the kink instability. A magnetic island is formed due to the helical distortion of the magnetic axis. This island then moves toward the central position while the flux surfaces originally placed around the magnetic axis are gradually pushed outward. A localized magnetic reconnection layer can be observed in the region where the inner flux surfaces come into contact with the outer flux surfaces. This is indicated in the small box drawn in Fig. 8 (a). After a reconnection process, a system with axisymmetric nested flux surfaces is recovered (see Fig. 8 (e)).

The Poincaré maps showing the evolution of the $\alpha = -0.6$ case can be observed in Fig. 9. The overall behavior is analogous to the previously studied case. A magnetic island is formed at an outer position (relative to the magnetic axis) which then moves and occupies

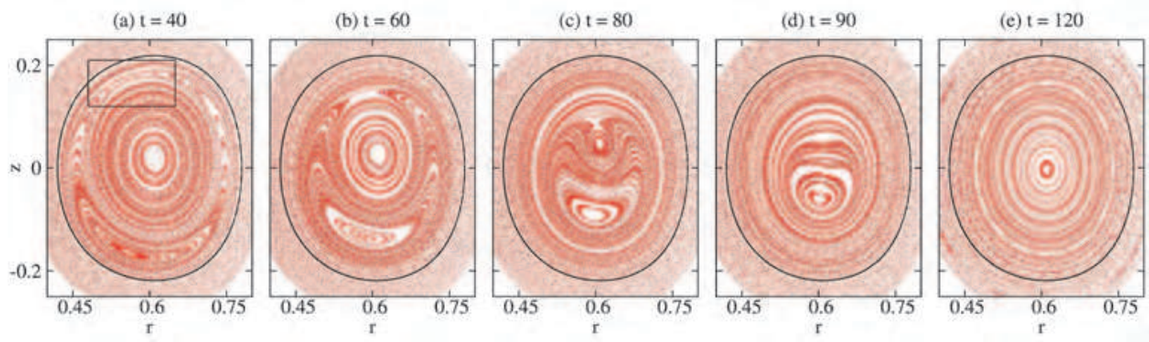

Fig. 8. Poincaré maps at several times showing the evolution of kink instability for the $\alpha = -0.4$ case. The black contour shows the initial position of the $q = 1$ surface.

the magnetic axis position. However, in this case a large region of stochastic magnetic field lines emerges between the two magnetic o-points and we are no longer able to identify a well defined localized reconnection layer.

The situation is even more drastic in the case with $\alpha = -0.7$ shown in Fig. 10. Most of the initially regular surfaces are quickly destroyed and large regions of stochastic field lines are observed. Though, a small coherent structure can still be devised even at times of strong activity (the saturation of the instability takes place at $t = 100$). After the instability saturation the toroidal modes decay and new regular nested flux surfaces are formed ($t = 200$).

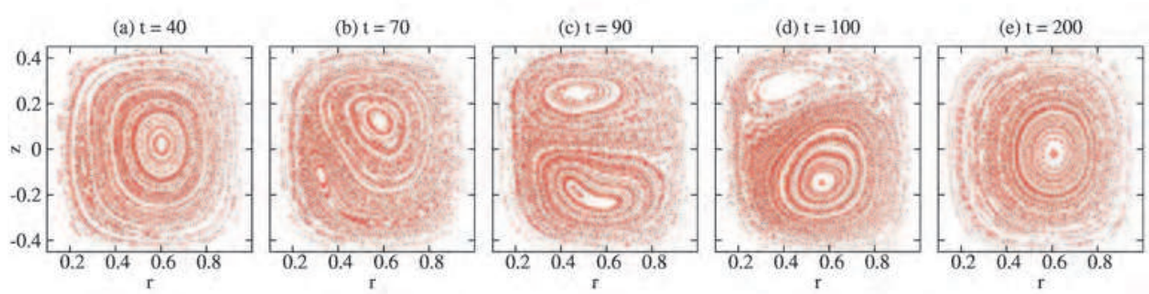

Fig. 9. Poincaré maps showing the evolution of the kink instability in the $\alpha = -0.6$ case.

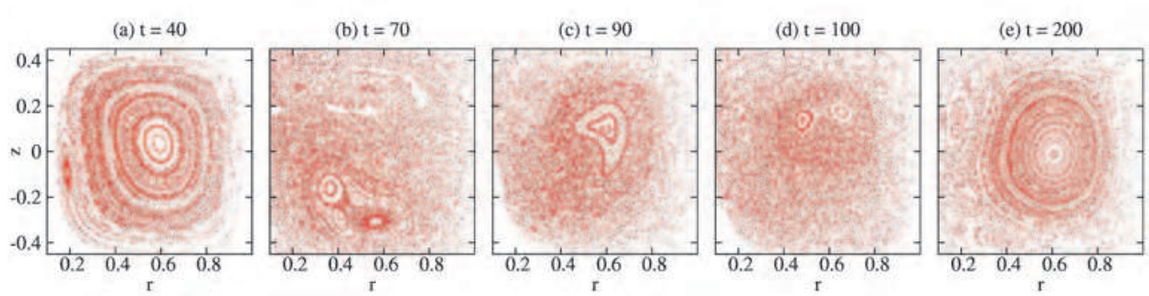

Fig. 10. Poincaré maps showing the evolution of the kink instability in the $\alpha = -0.7$ case.

In contrast with the marginally unstable case analyzed previously ($\alpha = -0.4$) where the activity was milder, here the larger level of fluctuations causes the field lines to wander through the whole domain. This facilitates the helicity transfer and enable a more effective flattening of the $\lambda(\psi)$ profile (as shown in Fig. 7).

It is important to keep in mind that these stochastic regions can be produced even by relatively low wave number magnetic fluctuations. In fact, few toroidal Fourier modes with a rather gentle dependence along the poloidal plane are enough to produce the disorder observed in Fig. 10 (d).

These observations are in agreement with the discussion presented in Sec. 4.2. As remarked there, a significant amount of small scale MHD activity (fluctuations) leading to the formation of numerous small current sheets is required to obtain the full relaxation behavior. In the marginal unstable case ($\alpha = -0.4$) the dominant kink mode produce a regular evolution in which a single localized current sheet is observed. This is not enough to produce a complete relaxation behavior with uniform λ in the final state, as it can be observed in Fig. 11.

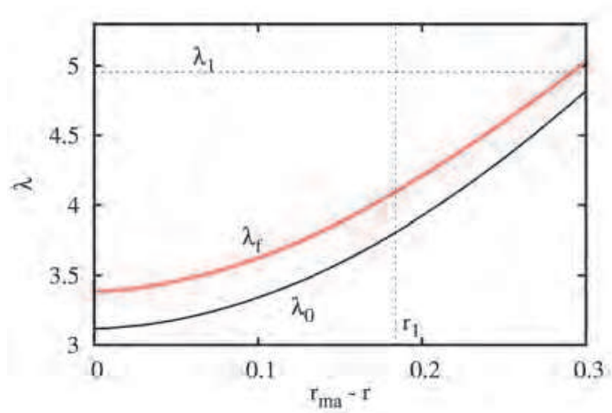

Fig. 11. λ profiles at $t = 0$ (λ_0) and at $t = 100$ (after reconnection, λ_f). In this plot the abscissa measures the distance to the magnetic axis. A partial relaxation behavior is evident, since λ_f is still far away from the eigenvalue λ_1.

As α is lowered (λ profile is steepened), the kink mode becomes stronger and activates higher order modes. Only when a significant level of activity is induced the Taylor's relaxation theory becomes applicable to obtain a good approximation of the final state of the system. Interestingly, the full relaxation behavior is recovered even for a modest separation of scales (Garcia-Martinez & Farengo, 2009a);(Garcia-Martinez & Farengo, 2009b).

5.3 Kink onset and resonant surfaces

Now we focus on the partial relaxation behavior of the marginally kink unstable configurations where relaxation theory is not applicable. A very useful concept developed in the context of the study of MHD modes (in particular the kink mode) is the safety factor q. The safety factor is the number of times a field line on a flux surface goes around toroidally

for a single poloidal turn. Based on the equation for a field line

$$\frac{rd\theta}{ds} = \frac{B_\theta}{B_p} \tag{51}$$

where ds is the distance in the poloidal direction while moving a toroidal angle $d\theta$, the safety factor can be defined as

$$q = \frac{1}{2\pi} \oint \frac{1}{r} \frac{B_\theta}{B_p} ds \tag{52}$$

where the integral is taken over a single poloidal circuit. Note that q adopts the same value for every field line lying on the same flux surface and thus it is a flux function $q = q(\psi)$. In

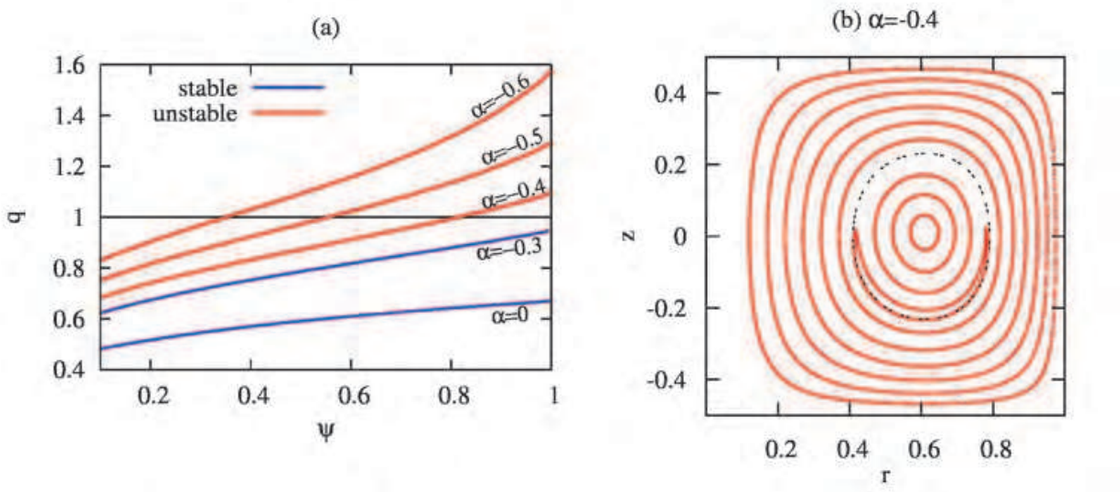

Fig. 12. (a) Safety factor profiles for several configurations. Note that configurations having a $q = 1$ surface are unstable. (b) Poincaré map showing ten field lines during the instability onset in the $\alpha = -0.4$ case. The dashed line shows the $q = 1$ surface, where the formation of a magnetic island is observed.

Fig. 12 (a) the q profiles for several configurations are shown. We already mentioned that the kink instability threshold lies between $\alpha = -0.3$ and $\alpha = -0.4$. In Fig. 12 (a) we can see that the kink instability is associated to the appearance of a rational surface with $q = 1$. Rational surfaces are those where $q = m/n$ being m and n integer numbers and thus q has a rational value. The field lines lying in such surfaces can not span a closed toroidal surface and are particularly prone to develop different MHD modes. That is why these surfaces are also called resonant surfaces. In Fig. 12 (b) we clearly see that it is at the $q = 1$ surface where the first modification to the flux surfaces occurs. This crescent shaped structure (which shows the onset of the island observed in Fig. 8) has a $n = 1$ toroidal dependence.

Note that, in the $\alpha = -0.4$ case, all the relevant MHD activity triggered by the kink takes place inside the $q = 1$ surface of the initial condition (Fig. 8). Thus, we can not expect this evolution to cause a complete relaxation process. However, some partial relaxation occurs due to the

magnetic reconnection of flux surfaces having different λ values, as confirmed in Fig. 11. The magnetic reconnection process is further studied in the next Section.

5.4 Magnetic reconnection process

Here we describe the magnetic reconnection process that redistributes currents in the case with $\alpha = -0.4$. Consider the Poincaré map inside the box shown in Fig. 8 (a). This is

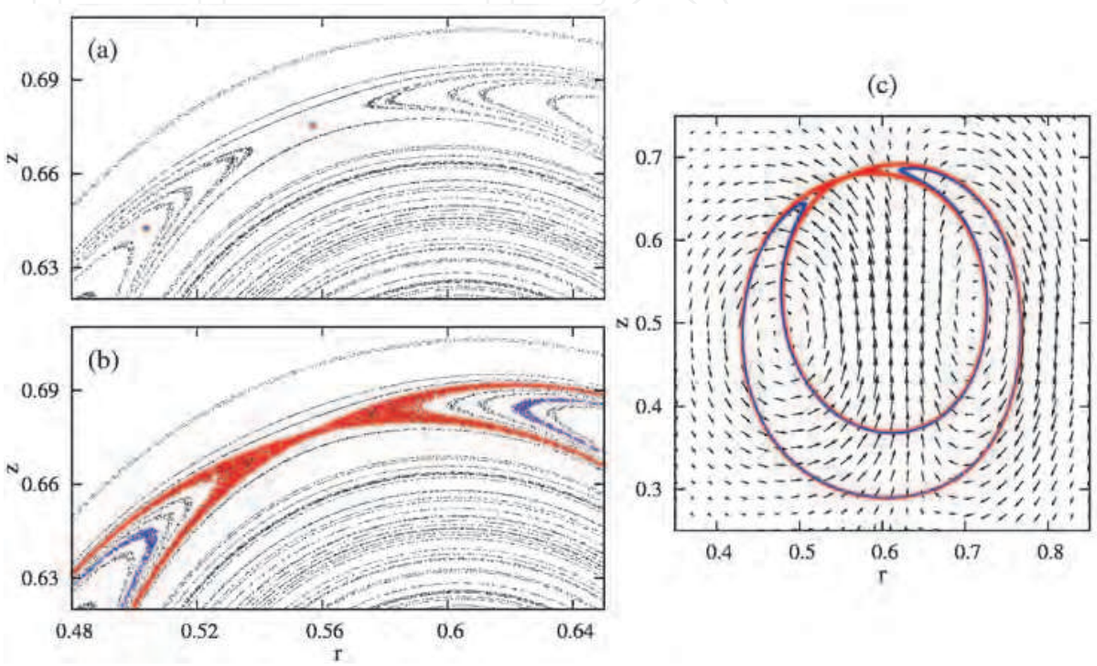

Fig. 13. (a) Poincaré map inside the box shown in Fig.8 (a). Two points, one red and one blue, are manually selected. (b) The same Poincaré plot including two additional magnetic lines followed from the selected points. (c) $n = 1$ component of the poloidal velocity (black vectors) and the two field lines also shown in (b).

shown in Fig. 13 (a). A reconnection layer is clearly identified, in the middle of which we have drawn a point (in red). We follow the magnetic field line that passes through this point for a long distance (ten thousand times the cylinder radius). The results for this single line are shown in Fig. 13 (b) and (c) (the red points) and in Fig. 14. The flow induced by the instability, shown with vectors in Fig. 13 (c), produces the helical distortion of the central flux surfaces. Eventually, one (or more) of these surfaces gets in contact with an outer surface. This is clearly observed in Fig. 14 where a single field line spans both surfaces. Note that the inner surface has a lower λ value than the outer one. At the helical reconnection layer λ adopts an intermediate value.

As a result of this reconnection a new magnetic structure is formed. This structure has a crescent shape cross section as shown by the blue dots in Fig. 13 (b) and (c). This is basically the closed surface that encloses the volume between the two reconnecting toroidal flux surfaces. Fig. 15 shows another visualization of this new magnetic entity. It has been constructed by following the magnetic field line that passes through the blue point indicated in Fig. 13 (a). It is interesting to note that this surface has a lower λ value in its inner face

Fig. 14. A single magnetic field line showing two reconnecting flux surfaces. Its color is proportional to the local λ value (the color scale is indicated on right). The outer surface has a higher λ than the inner surface. The helical reconnection layer adopts an intermediate value.

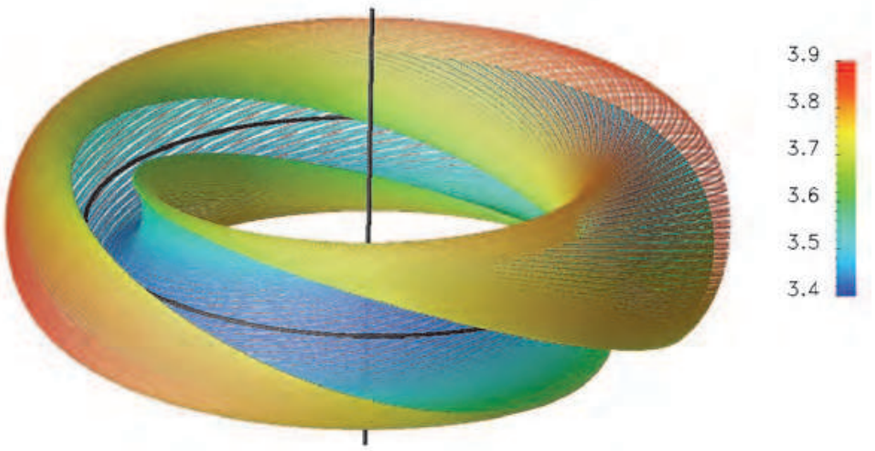

Fig. 15. Magnetic structure formed by the reconnection of the flux surfaces shown in Fig. 14. The color scale indicates local λ value.

(corresponding to the λ value of the original inner flux surface) and a higher λ value in its outer face. This clearly shows that the reconnection is a localized process. It is also evident that the mean λ value of this structure will lie between the λ values of the original surfaces.

With these considerations in mind we can reinterpret Fig. 8. The motion of the island toward the magnetic axis involves the reconnection of inner and outer surfaces having low and high λ values, respectively. The new surfaces formed adopt intermediate λ values. The result of this redistribution is shown in Fig. 11. Note that all this activity takes place in the region where $\psi \geq 0.8$ (the region inside the original location of the $q = 1$ surface). In Fig. 6 (a) we see that within this region $\lambda \lesssim 4$ and thus we can not expect a full relaxation process.

A final comment is made regarding the symmetry of this process. The kink mode has a $n = 1$ toroidal dependence and thus the reconnection layer shown in Fig. 13 has a dominant helical shape. However, we want to mention that there are also higher harmonics ($n > 1$) present in the reconnection process. This can be observed in Fig. 16 where the inner flux surface of Fig. 14 is shown. The high λ region (mainly yellow) shows the reconnection layer. It

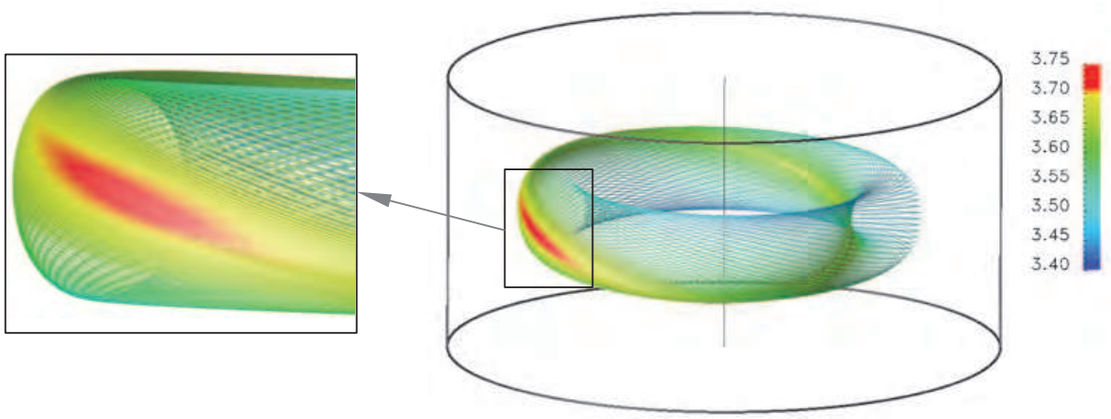

Fig. 16. Inner reconnecting magnetic flux surface. A zoom near the zone of higher λ value reveals the presence of higher toroidal harmonics ($n > 1$).

has a mainly helical structure, however, a zoom around the region with the highest λ values (shown in red) reveals the presence of higher toroidal components. It is not clear, at this point, if higher harmonics play an important role or this process could be recovered considering a two dimensional problem with helical symmetry.

5.5 Reconnection model for the resistive kink mode

The magnetic reconnection process described so far leads to a flux rearrangement in the region where $q > 1$. This process involves a rather regular evolution of the magnetic surfaces with only one helical current sheet. Without a significant level of MHD activity the magnetic relaxation theory becomes inapplicable. Now we seek for a simple but adequate model to describe the final state of the non-linear evolution of the resistive kink.

In the context of tokamak research, the evolution of the resistive kink has been intensively studied. In particular, it is believed that this mode is responsible for a phenomenon called *sawtooth oscillations* that limits in practice the maximum temperature reachable at the core. One of the first models to describe the final state of the non linear resistive kink mode was proposed by Kadomtsev (1975) (see also the explanation of Wesson (2004)). In this Section we describe the Kadomtsev's model and discuss its applicability to the results of our simulations. Then, a modification to the model that significantly improves the agreement with our results will be introduced.

The magnetic field lines on the $q = 1$ surface form a helix around the magnetic axis. The Kadomtsev's model describes the reconnection process in terms of the flux perpendicular to this helix, called helical flux ψ_h. This flux can be computed from the helical magnetic field

$$B_h = B_z(1 - q) \tag{53}$$

as

$$\psi_h(r) = 2\pi \int_r^{r_{\mathrm{ma}}} B_z(x, z_{\mathrm{ma}})(1 - q)x dx \tag{54}$$

where (r_{ma}, z_{ma}) is the position of the magnetic axis and this definition is to be used with $r \leq r_{ma}$. In what follows we will use the minor radius $\tilde{r} = r_{ma} - r$ as the abscissa. In order to

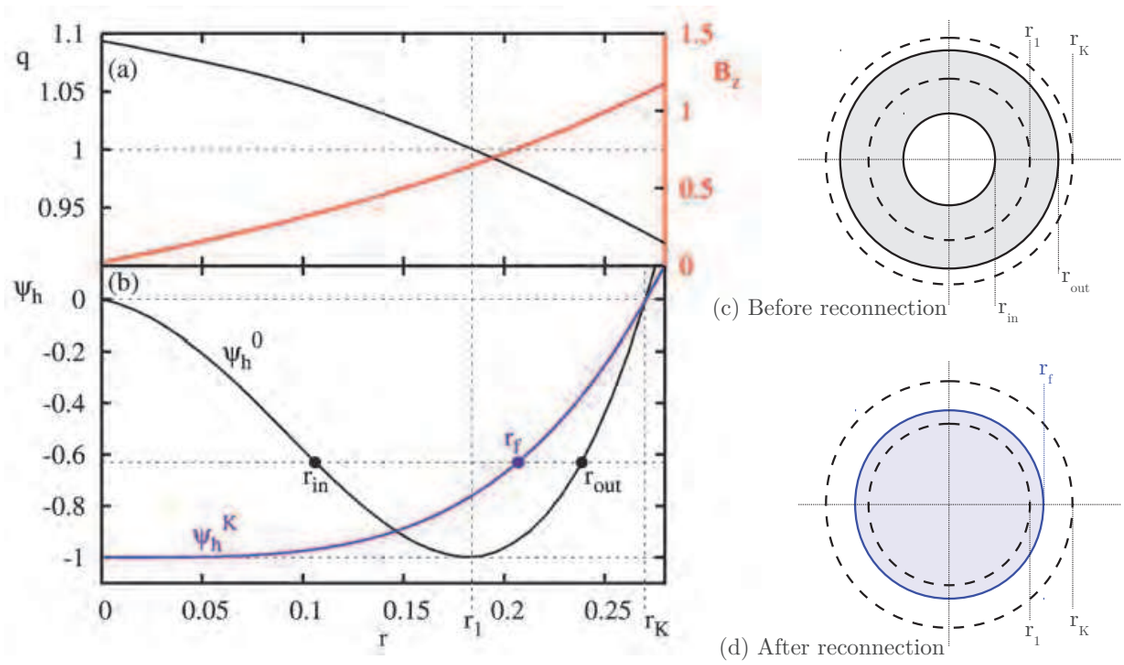

Fig. 17. (a) Initial q and poloidal field (B_z) profiles. (b) Initial (ψ_h^0) and final (ψ_h^K) helical flux predicted by Kadomtsev's model. ψ_h^K is obtained by assuming that the area enclosed by the two reconnecting surfaces before reconnection (c) is equal to the area inside the final reconnected surface (d).

not overload the notation we will drop the tilde. Fig. 17 (a) shows q and B_z as a function of the minor radius. Note that B_h changes its sign at r_1, where $q = 1$, producing a minimum in ψ_h^0 as shown in Fig. 17 (b). The Kadomtsev's model model provides a simple way to compute the helical flux after reconnection ψ_h^K (see Fig. 17 (b)) from which one can readily obtain the reconnected poloidal field profile.

The reconnection begins at the minimum value of ψ_h^0, i.e. at $\psi_h^0(r_1)$. It is assumed that this flux surface will form the new centre of the plasma and thus $\psi_h^K(0) = \psi_h^0(r_1)$. The reconnection then proceeds merging each pair of flux surfaces having the same ψ_h value. In the particular example of Fig. 17, the flux surfaces initially located at r_{in} and r_{out} will reconnect forming a new flux surface at r_f. The position of the final surface r_f is given by toroidal flux conservation. Assuming that the toroidal field does not change during the process, the area enclosed by the two initial surfaces should be equal to the area inside the final surface (see Fig. 17 (c) and (d)). This means that

$$r_f^2 = r_{out}^2 - r_{in}^2 \tag{55}$$

where we have simplified the problem by considering flux surfaces with circular cross section. The reconnection process ends at $\psi_h = 0$ so that the flux surfaces located outside r_K remain unaffected.

Several aspects of this model are in close agreement with the evolution of the marginally unstable case shown in Fig. 8. First of all, the fact that the reconnection process is restricted to the core, i.e. the region $q \lesssim 1$, and does not affect the whole configuration (as assumed by relaxation theory). Secondly, in Fig. 8 we effectively see that the small island formed at r_1 ($q = 1$) moves until it occupies the position of the magnetic axis. Thirdly, in our simulation we also observe what is called a complete reconnection process. Note that since ψ_h^{K} is monotonic this means that B_h after reconnection does not change its sign. This means in turn that q does not cross 1 (in fact q is equal to 1 at $r = 0$). The absence of $q = 1$ surfaces prevents the appearance of magnetic islands just after the reconnection and thus it is said that the Kadomtsev's model predicts complete reconnection. Accordingly, we do not observe any island (other that the magnetic axis) after the reconnection (see Fig. 8) and the resulting q profile does not cross 1, as observed in Fig. 18 (a). Despite this agreement in the overall

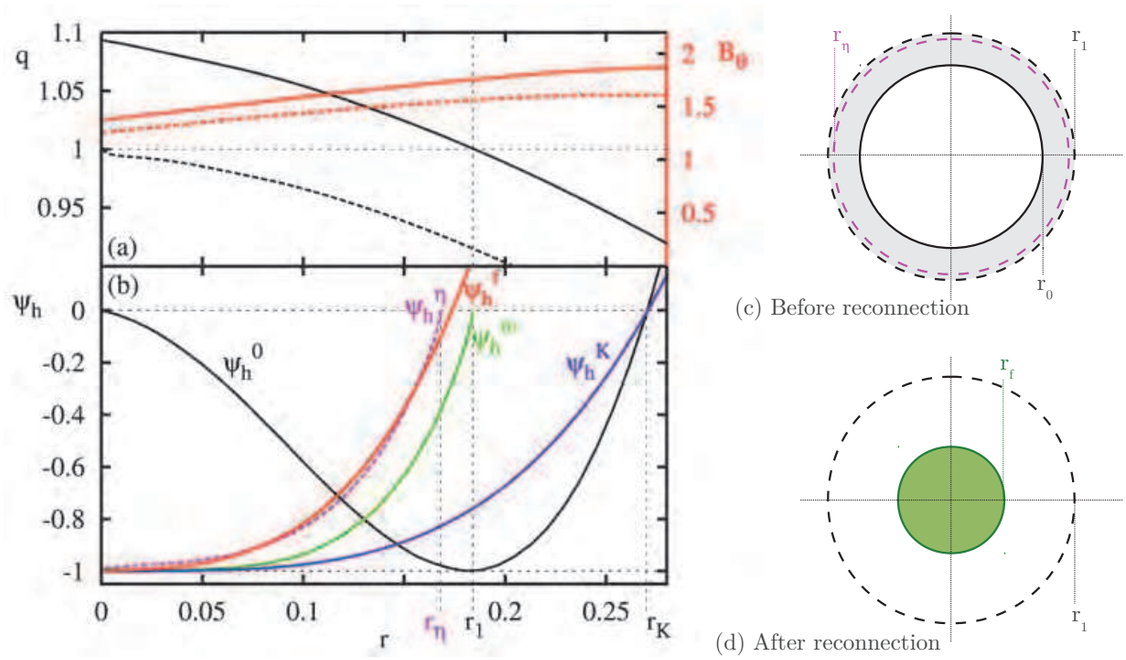

Fig. 18. (a) Initial (solid) and reconnected, i.e. at $t = 100$, (dashed) q and toroidal field profiles. (b) Several helical fluxes profiles: initial (ψ_h^0), final (ψ_h^{f}), predicted by Kadomtsev (ψ_h^{K}), predicted by the modified model (ψ_h^{m}) and predicted by the modified model with correction due to resistive decay (ψ_h^{η}). The modified model proposed involves the reconnection of the surface at r_0 (c) with the surface at r_{f} (d). The shaded regions have the same area.

behavior we will show that the results of the $\alpha = -0.4$ case are better described by introducing a modification to the Kadomtsev's model. In Fig. 18 (b) the initial helical flux ψ_h^0 and the final ψ_h^{K} predicted by Kadomtsev are compared with the actual final helical flux ψ_h^{f} (the red curve) obtained at $t = 100$ for the $\alpha = -0.4$ case. Note that the agreement is not good.

A better approximation can be obtained by looking at Fig. 8 more carefully and noting that the reconnection process takes place *inside* the $q = 1$ surface. Since little or no effect is observed outside r_1 we propose a modified procedure for the construction of the reconnected helical flux ψ_h^{m}. Again, the flux surface at r_1 is reconnected with the magnetic axis so $\psi_h^{\mathrm{m}}(0) = \psi_h^0(r_1)$.

Then, the flux surface initially placed at r_0, see Fig. 18 (c), reconnects and ends at r_f , Fig. 18 (d), in such a way that

$$r_\mathrm{f}^2 = r_1^2 - r_0^2 \tag{56}$$

which expresses the conservation of the area of the shaded regions of Fig. 18 (c) and (d). With the initial helical flux ψ_h^0 and Eq. (56) it is possible to compute the reconnected helical flux predicted by the modified model ψ_h^m. This is shown by the green curve of Fig. 18 (b). While this prediction is much closer than the Kadomtsev's model to the actual final state there is still a significant difference. In what follows we will show that this difference is due to resistive dissipation.

Relations (55) and (56) express the toroidal flux conservation assuming that it does not decay, i.e. the toroidal fluxes inside r_K and r_1 do not change. However, as can be observed in Fig. 18 (a), the toroidal magnetic field is visibly reduced due to resistivity. One way to take into account this resistive decay is to change the reference radius with which we make the construction of ψ_h^m given by Eq. (56). In particular, we define r_η as the radius of the circle that contains at $t = 0$ the same amount of toroidal flux that is contained inside r_1 at $t = 100$. If we now compute the reconnected helical flux using Eq. (56) but changing r_1 by r_η we obtain ψ_h^η, shown by the dashed line of Fig. 18 (b). The agreement with the actual final helical flux is very good and this suggests that the modified model indeed captures the basic physics of the reconnection process.

6. Conclusions

In this Chapter we have presented a general picture of the magnetic confinement of high temperature plasmas. This has motivated the introduction of the MHD model which provides an adequate framework to study the macroscopic dynamics of fully ionized plasmas. We have focused our attention on the physical mechanism called plasma relaxation. In particular we have studied the magnetic relaxation process driven by the kink instability in spheromak configurations.

Experiments as well as previous theoretical works showed the existence of a partial relaxation behavior for marginally unstable configurations (they do not evolve toward the minimum energy state). This is in contrast to the well established relaxation theory that states that the plasma should relax to the minimum energy configuration. In this work we have explored these two regimes, namely complete relaxation and partial relaxation, by varying the slope of the initial $\lambda(\psi)$ profile. This controls the degree of instability of the initial configuration as well as the position of the rational surface having safety factor equal to one. The relevance of the position of this rational (or resonant) surface to the partial relaxation behavior was discussed. In particular, we showed that in marginally unstable cases this surface is not far from the magnetic axis and the MHD activity during relaxation remains inside this resonant surface (which is no longer resonant after relaxation). These results suggest that the $q = 1$ surface plays a major role in the evolution of spheromaks during sustainment because in that situation they operate around the kink instability threshold.

The analysis of more unstable cases showed that the full relaxation process predicted by the relaxation theory is only achieved when the magnetic fluctuations produce stochastic field line regions of size comparable of that of the whole system. This result clearly indicates that

the relaxation theory as formulated by Taylor (1974) is applicable to highly unstable plasmas but it becomes useless to study the operation of configurations near an instability threshold.

The kink instability produces the helical deformation of the flux surfaces near the magnetic axis. This drives the reconnection of the inner flux surfaces with the outer ones. This process has been studied in detail. The reconnection layer has been identified as well as the new structure resulting from the reconnection of the two flux tubes. Taking the low (high) λ value of the inner (outer) tube on its inner (outer) side, these crescent shaped structures average the λ value inside the $q = 1$ surface. Even when the flux surfaces remain regular during this evolution, the process involves the full reconnection of all the magnetic tubes inside the $q = 1$ surface. This is of course undesired from the point of view of confinement and could partially explain the poor performance of spheromak operation (compared to tokamaks and RFP's). However further studies are required on this topic regarding the coupled dynamics between the kink and the external driving of the system. This could be done by applying appropriate boundary conditions to model the injection of helicity from a source (Garcia-Martinez & Farengo, 2010).

Finally, models for the reconnection process driven by the kink mode were discussed. The Kadomtsev's model was presented and showed to give a poor description of the actual simulation results. A modification to this model that greatly improves the agreement with simulations was proposed. A method to incorporate the correction due to the resistive decay of the configuration was described.

7. References

Bellan, P. (2000). *Spheromaks: a practical application of magnetohydrodynamic dynamos and plasma self-organization*, Imperial College Press, London.

Biskamp, D. (2000). *Magnetic reconnection in plasmas*, Cambridge University Press, Cambridge/New York.

Braginskii, S. (1965). Transport processes in a plasma, *Reviews of Plasma Physics*, 1: 205-311.

Finn, J. & Antonsen, T. (1985). Magnetic helicity: what it is, and what it is good for?, *Comments Plasma Phys. Controlled Fusion*, 33: 1139.

Friedberg, J. (1987). *Ideal MHD*, Plenum Press, New York.

Garcia-Martinez, P. & Farengo, R. (2009a). Selective decay in a helicity-injected spheromak, *J. Phys.: Conf. Ser.*, 166: 012010.

Garcia-Martinez, P. & Farengo, R. (2009b). Non-linear dynamics of kink-unstable spheromak equilibria, *Phys. Plasmas*, 16: 082507.

Garcia-Martinez, P. & Farengo, R. (2010). Spheromak formation and sustainment by tangential boundary flows, *Phys. Plasmas*, 17: 050701.

Hasegawa , A. (1985). Self-organization processes in continuous media, *Adv. Phys.*, 34: 1-42.

Heyvaerts J. & Priest, E. (1984). Coronal heating by reconnection in DC current systems: a theory based on Taylor's hypothesis. *Astron. Astrphys.*, 137: 63-78.

Jarboe, T. (2005). The spheromak confinement device, *Phys. Plasmas*, 12: 058103.

Kadomtsev, B. (1975). Disruptive instabilities in tokamaks, *Sov. J. Plasma Phys.*, 1: 389-391.

Kitson, D. & Browning, P. (1990). Partially relaxed magnetic field equilibria in a gun-injected spheromak, *Plasma Phys. Controlled Fusion*, 32 (14): 1265-1287.

Knox, S., Barnes, C., Marklin, G., Jarboe, T., Henins, I., Hoida, H. & Wright, B. (1986). Observations of spheromak equilibria which differ from the minimum-energy state and have internal kink distortions, *Phys. Rev. Lett.*, 56: 842-845.

Moffat, H. (1978). *Magnetic field generation in electrically conducting fluids*, Cambridge University Press, London/New York.

Montgomery, D., Turner, L. & Vahala, H. (1978). Three-dimensional magnetohydrodynamic turbulence in cylindrical geometry. *Phys. Fluids*, 21: 757-764.

Priest, E. & Forbes, T. (2000). *Magnetic reconnection: MHD theory and applications*, Cambridge University Press, New York.

Rosenbluth, M. & Bussac, M. (1979). MHD stability of spheromak, *Nuc. Fusion*, 19: 489-498.

Taylor, J. (1974). Relaxation of toroidal plasma and generation of reverse magnetic fields, *Phys. Rev. Lett.*, 33: 1139-1141.

Taylor, J. (1986). Relaxation and magnetic reconnection in plasmas, *Rev. Mod. Phys.*, 58: 741-763.

Wesson, J. (2004). *Tokamaks (Third Edition)*, Clarendon Press - Oxford, New York.

Willett, D., Browning, P., Woodruff, S. & Gibson, K. (1999). The internal magnetic structure and current drive in the SPHEX spheromak, *Plasma Phys. Controlled Fusion*, 41: 595-612.

Woltjer, L. (1958). A theorem on force-free magnetic fields, *Proceedings of the National Academy of Science*, 44: 489-491.

Zheng, L. & Furukawa, M. (2010). Current-interchange tearing modes: Conversion of interchange-type modes to tearing modes, *Phys. Plasmas*, 17: 052508.

IntechOpen

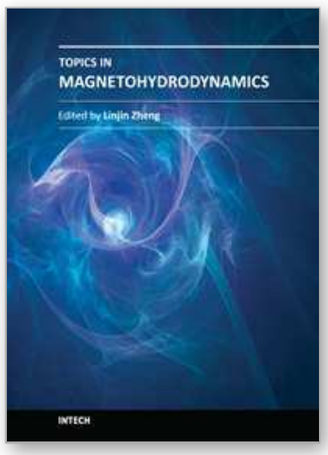

Topics in Magnetohydrodynamics

Edited by Dr. Linjin Zheng

ISBN 978-953-51-0211-3
Hard cover, 210 pages
Publisher InTech
Published online 09, March, 2012
Published in print edition March, 2012

To understand plasma physics intuitively one need to master the MHD behaviors. As sciences advance, gap between published textbooks and cutting-edge researches gradually develops. Connection from textbook knowledge to up-to-dated research results can often be tough. Review articles can help. This book contains eight topical review papers on MHD. For magnetically confined fusion one can find toroidal MHD theory for tokamaks, magnetic relaxation process in spheromaks, and the formation and stability of field-reversed configuration. In space plasma physics one can get solar spicules and X-ray jets physics, as well as general sub-fluid theory. For numerical methods one can find the implicit numerical methods for resistive MHD and the boundary control formalism. For low temperature plasma physics one can read theory for Newtonian and non-Newtonian fluids etc.

How to reference
In order to correctly reference this scholarly work, feel free to copy and paste the following:

Pablo L. Garcia-Martinez (2012). Dynamics of Magnetic Relaxation in Spheromaks, Topics in Magnetohydrodynamics, Dr. Linjin Zheng (Ed.), ISBN: 978-953-51-0211-3, InTech, Available from: http://www.intechopen.com/books/topics-in-magnetohydrodynamics/dynamics-of-magnetic-relaxation-in-spheromaks

INTECH
open science | open minds

InTech Europe
University Campus STeP Ri
Slavka Krautzeka 83/A
51000 Rijeka, Croatia
Phone: +385 (51) 770 447
Fax: +385 (51) 686 166
www.intechopen.com

InTech China
Unit 405, Office Block, Hotel Equatorial Shanghai
No.65, Yan An Road (West), Shanghai, 200040, China
中国上海市延安西路65号上海国际贵都大饭店办公楼405单元
Phone: +86-21-62489820
Fax: +86-21-62489821

© 2012 The Author(s). Licensee IntechOpen. This is an open access article distributed under the terms of the Creative Commons Attribution 3.0 License, which permits unrestricted use, distribution, and reproduction in any medium, provided the original work is properly cited.

IntechOpen

IntechOpen